ELSEVIER

Journal of Structural Geology 29 (2007) 2006–2016

JOURNAL OF STRUCTURAL GEOLOGY

www.elsevier.com/locate/jsg

Mesozoic structural architecture of the Lang Shan, North-Central China: Intraplate contraction, extension, and synorogenic sedimentation

Brian J. Darby [a,*], Bradley D. Ritts [b,1]

[a] *Department of Geology and Geophysics, Louisiana State University, Baton Rouge, LA 70803, USA*
[b] *Chevron Energy Technology Company, 6001 Bollinger Canyon Road, San Ramon, CA 94583, USA*

Received 17 November 2006; received in revised form 20 June 2007; accepted 24 June 2007
Available online 28 July 2007

Abstract

The Lang Shan, North-Central China, has experienced a complex Mesozoic to recent history of intraplate deformation and sedimentation. Well-exposed cross-cutting relationships document Jurassic right-lateral strike-slip faulting (transtension) followed by several tens of kilometers of Late Jurassic to Early Cretaceous north-northwest–south-southeast crustal shortening and development of an associated foreland basin. Since the Early Cretaceous, the south-central Lang Shan has undergone two phases of extension. The first, which occurred along north–south oriented structures, may represent collapse of an overthickened crust. The youngest deformation is represented by the active Cenozoic mountain-front normal fault system. This compound history may be the result of the complicated far-field effects of plate interactions combined with structural inheritance in a region adjacent to a rigid and undeformed crustal block, the Ordos block.

Keywords: Intraplate; China; Fold-thrust belt; Foreland basin; Continental extension; Ordos; Inner Mongolia; Yinshan

1. Introduction

The diffuse nature of plate boundaries has been documented over the nearly four decades since plate tectonic theory was proposed (see review by Gordon, 1998). The nature of how these diffuse, or intraplate zones, accommodate plate convergence is critical to understand the processes by which continents grow and subsequently deform. Intraplate belts of deformation provide key insights into the far-field effects of plate boundary interactions—those plate boundaries may now only be preserved as complex suture zones. In addition, intraplate belts and the associated sedimentary basins record a long and complex history of deformation (e.g. Teyssier, 1985; Kluth, 1986; Shaw et al., 1991; Hendrix et al., 1992; Ziegler et al., 1995, 1998; Sandiford and Hand, 1998; Darby et al., 2001; Davis et al., 2001; Ritts et al., 2001, 2004; Darby and Ritts, 2002; Johnson, 2004; Cope et al., 2005). Understanding these histories may afford the opportunity to better understand problems ranging from the reactivation of mechanical heterogeneities to development of large, non-marine sedimentary basins (Ziegler et al., 1998; Sandiford and Hand, 1998; Hand and Sandiford, 1999; Ritts et al., 2001, 2004; Darby and Ritts, 2002; Cope et al., 2005).

Asian, more specifically, Chinese examples of intraplate deformation have long been discussed in the geologic literature (e.g. Wong, 1929) and have recently begun to receive more attention (e.g. Hendrix and Davis, 2001). These intraplate belts of deformation may play a critical role in understanding the tectonic evolution of China and Asia including use as both passive strain markers and controlling features of younger, Himalayan–Tibetan structures especially given recent documentation of large-scale Cenozoic left-lateral strike-slip faulting beyond the margins of the Northern Tibetan

* Corresponding author. Present address: ExxonMobil Upstream Research Company, P. O. Box 2189, Houston, TX 77252-2189, USA. Tel.: +1 225 578 5810; fax: +1 225 578 2302.
E-mail addresses: brian.j.darby@exxonmobil.com (B.J. Darby), Bradley Ritts@chevron.com (B.D. Ritts).
[1] Tel.: +1 812 856 0307; fax: +1 812 855 7899.

0191-8141/$ - see front matter © 2007 Elsevier Ltd. All rights reserved.
doi:10.1016/j.jsg.2007.06.011

Plateau (Darby et al., 2005; Webb and Johnson, 2006). Despite their importance for understanding continent evolution, the spatial and temporal distribution of pre-Cenozoic intraplate mountain belts in northern China remains unresolved.

The Lang Shan (Fig. 1), in the northwest corner of the Ordos Plateau (Fig. 1), contains a spectacular example of late Mesozoic intraplate crustal shortening and subsequent collapse with associated synorogenic sedimentation. We present new data that illustrate the structural architecture, document cross-cutting relationships, constrain the timing of deformation, and a thrust belt restoration from this poorly studied area. This study area is significant in that it provides additional constraints on the spatial extent and magnitude of Mesozoic intraplate deformation in China. Because the long-term structural evolution of this belt was accompanied at each stage by syntectonic sedimentation, the Lang Shan also provides an excellent record to the changing surficial environments that accompanied growth and decay of this intracontinental mountain belt.

2. Rock units and stratigraphy

2.1. Precambrian

Precambrian rock units in the Lang Shan were not differentiated by the authors. They consist mainly of foliated metasedimentary units such as quartzite, schist, and marble. Other basement lithologies include gneiss and some granitic plutons, some of which are foliated. Precambrian crystalline rocks, along with younger plutons, make up the majority of the rugged Lang Shan.

2.2. Late Paleozoic–Triassic granitoid plutons

A regionally extensive Late Paleozoic–Triassic (NMBGMR, 1999) batholith is well exposed in the central portion of the range (Fig. 2). The NMBGMR (1999) dated several of these plutons (U-Pb, zircon) and report ages from 292.3 to 205.1 Ma. Plutons in the batholith are mainly granites (quartz, grey to pink K-feldspar, plagioclase, and biotite) that lack a solid-state foliation. Outside the main batholith, several plutons intrude the Precambrian basement.

2.3. Jurassic Jr_u

The spatially largest exposure of Jurassic strata (Jr_u) in the south-central Lang Shan is a highly faulted, triangular-shaped exposure in the central portion of the study area (Fig. 2). These strata rest unconformably on crystalline basement along the southwestern margin of the exposure. The lower two-thirds of this exposure, which is at least 1 km thick, consist of boulder conglomerate (maximum clast size ~ 4 m) and sandstone. Conglomerate clasts include gneiss, granitoids, carbonate, and red sandstone. White carbonate sedimentary breccias are interbedded with brown sandstone and conglomerate along the southern exposure of this unit (N41°04.20′, E106°59′). These carbonate breccias only extend northward into the sedimentary section for a few tens of meters and have wedge-shaped geometries in cross-section that thicken and coarsen to the southeast. The source of the carbonate breccias is most likely the white marble found in the footwall of the normal fault that is locally preserved along the southeastern edge of the Jurassic section. The upper third of the section is a fine-grained sequence of buff to green sandstone, siltstone, and shale with minor

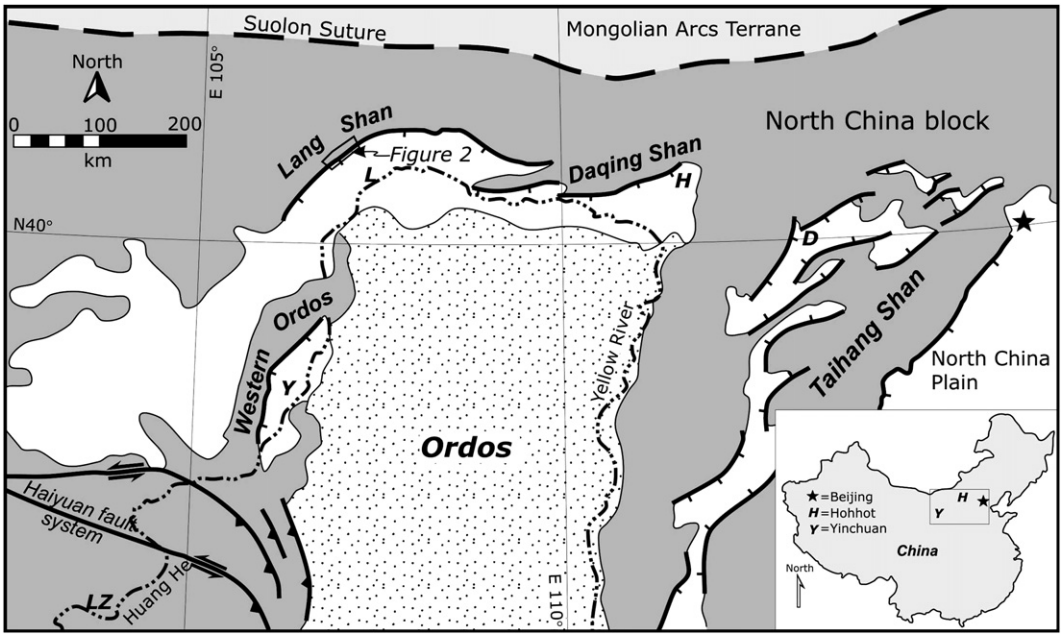

Fig. 1. Location map of the northern Ordos region, North China adopted from Darby and Ritts (2002). Light grey, Mongolian arcs terrane; medium grey, the Archean/Proterozoic-floored North China block; stippled pattern, the Ordos Plateau, formerly a Mesozoic basin; star, Beijing, D, Datong; H, Hohhot; L, Linhe; LZ, Lanzhou; Y, Yinchuan. Active structures adopted from Zhang et al. (1998). Note location of Fig. 2.

pebble conglomerate. The NMBGMR (1999) assigned an Early Cretaceous age on the basis of plant fossils for the uppermost, fine-grained portion of the section, although the authors were unable to confirm this age. We favor a Jurassic age for at least the lower conglomerate portion of the section based on the unit's structural history and sedimentology, discussed later. This interpretation is consistent with previous age assignments from Chinese studies (NMBGMR, 1991).

2.4. Latest Jurassic and Lower Cretaceous

Three Lower Cretaceous units (not including sub-units) are exposed along the central southeastern flank of the Lang Shan (Fig. 2).

2.4.1. Unit K_1A

The oldest of the Lower Cretaceous units, K_1A, is exposed along the south and east portions of the Lang Shan (Fig. 2). The unit has two members, K_1A_F (for ''foredeep'') and K_1A_W (for ''wedge-top''). Member K_1A_F consists of buff to red sandstone, buff to red cobble to boulder conglomerate, and lesser green to black shale. New palynology from this section yields a minimum Late Jurassic to Early Cretaceous age. Unit K_1A rests unconformably on Jurassic strata along the southwestern portion of the study area (Fig. 2). Conglomerate clast lithologies include non-foliated granitoids, basement schist and gneiss, and sandstone. It should also be noted that conglomerate compositions appear to be cyclical in nature—alternating from beds that are dominated by schist and gneiss to beds that are dominated by granitoids. The color of this unit changes gradually from tan sandstone and green mudstone near the base to red hues near the top. Its minimum thickness is 930 m. In general, the section displays a coarsening upwards grain size trend and changes from dominantly sandstone and lesser cobble conglomerate to mostly cobble- and boulder conglomerate and sandstone. This coarsening upwards is consistent with deposition in the foredeep depozone of a foreland basin system (e.g. DeCelles and Giles, 1996), an interpretation compatible with its structural setting.

This unit is intruded by a basalt sill (~10 m in width), which was collected for whole-rock Ar/Ar analysis. The basalt is interpreted to be a sill on the basis that both its upper and lower contacts with Lower Cretaceous sedimentary units show evidence of contact metamorphism and some small dikes. At least one small stopped block was also observed in the sill. Unfortunately, Ar/Ar analysis did not yield a useable age.

Member K_1A_F is overlain along an angular unconformity by member K_1A_W (Fig. 2). This higher unit is composed of dominantly boulder to cobble conglomerate and sandstone and contains growth strata in a piggyback basin and both progressive and buttress unconformities. As in the lower member of this unit, conglomerate clasts include non-foliated granitoids, basement lithologies, and some sandstone. Smaller basalt sills also intrude this unit. Member K_1A_W has a minimum thickness of ~750 m. The large clast size (up to 4 m) and presence of angular, buttress, and progressive unconformities within the K_1A_W section suggest that it is a synorogenic section with respect to the thrust and reverse faults that cut it (Figs. 2, 3). This unit is interpreted as the wedge-top depozone of a foreland basin system as defined by DeCelles and Giles (1996).

2.4.2. Unit K_1B

This Lower Cretaceous unit is predominantly exposed in a continuous ~35 km-long strip along or near the mountain-front in the south-central Lang Shan (Fig. 2). Several sub-members of this unit were distinguished while mapping but are extremely limited spatially and are therefore, not shown on the geologic map. Unit K_1B is comprised of red sandstone, pebble to boulder conglomerate, and mudstone, and lies in the footwall of a northwest-dipping thrust or reverse fault present for most of its exposed length (Figs. 2, 3). Conglomerate clast lithologies include Precambrian metasedimentary units such as quartzite, marble, and schist, gneiss, and granitoids. At some locales near the mountain-front the unit rests unconformably on Precambrian basement (Fig. 2). However, in southwest portions of the map area (Fig. 2), this unit sits atop unit K_1A_F along an angular unconformity (Fig. 2). At that local, unit K_1B is mostly sandstone and mudstone and the angularity between the two units is up to 90°. Locally, near thrust contacts, grain size coarsens to dominantly boulder-sized clasts and progressive unconformities can be found. The minimum thickness of this unit is 354 m, however, its true thickness may be similar to K_1A. Lower portions of K_1B may be the distal equivalents of the upper portions of member K_1A_F. As with unit K_1A, unit K_1B has the sedimentary characteristics of deposition in the foredeep depozone of a foreland basin (e.g. DeCelles and Giles, 1996).

2.4.3. Unit K_1C

Sedimentary unit K_1C is present only in a small area (~12 km^2) in the northeast portion of Fig. 2 and is entirely bordered by normal faults. Assigned an Early Cretaceous age by the NMBGMR (1999), it is composed of sandstone, conglomerate, and shale (Fig. 2). The color of this unit changes from dominantly dark grey and green near the base to buff/tan and red in higher portions of the section. Clasts in conglomerate intervals are dominantly gneiss, schist and non-foliated granitic rocks. This generally southeast-dipping sedimentary section fines upwards from predominantly boulder conglomerate and sandstone near its western and northern edges to mostly sandstone and mudstone in southern and eastern exposures. This section has a minimum thickness of 530 m. The relationships between unit K_1C and older units in the field area are not exposed.

3. Structural framework: Lang Shan fold-thrust belt and subsequent crustal extension

The well-exposed Lang Shan fold-thrust belt contains a complicated array of structural elements that include several thrust/reverse faults that involve basement and sedimentary units, large folds, strike-slip faults, and normal faults. Excellent exposure and access along the south-central portion of the Lang Shan allow for detailed observations of structures and cross-cutting relationships (discussed in Section 4). Several cross-sections were drawn through the south-central Lang Shan and are shown

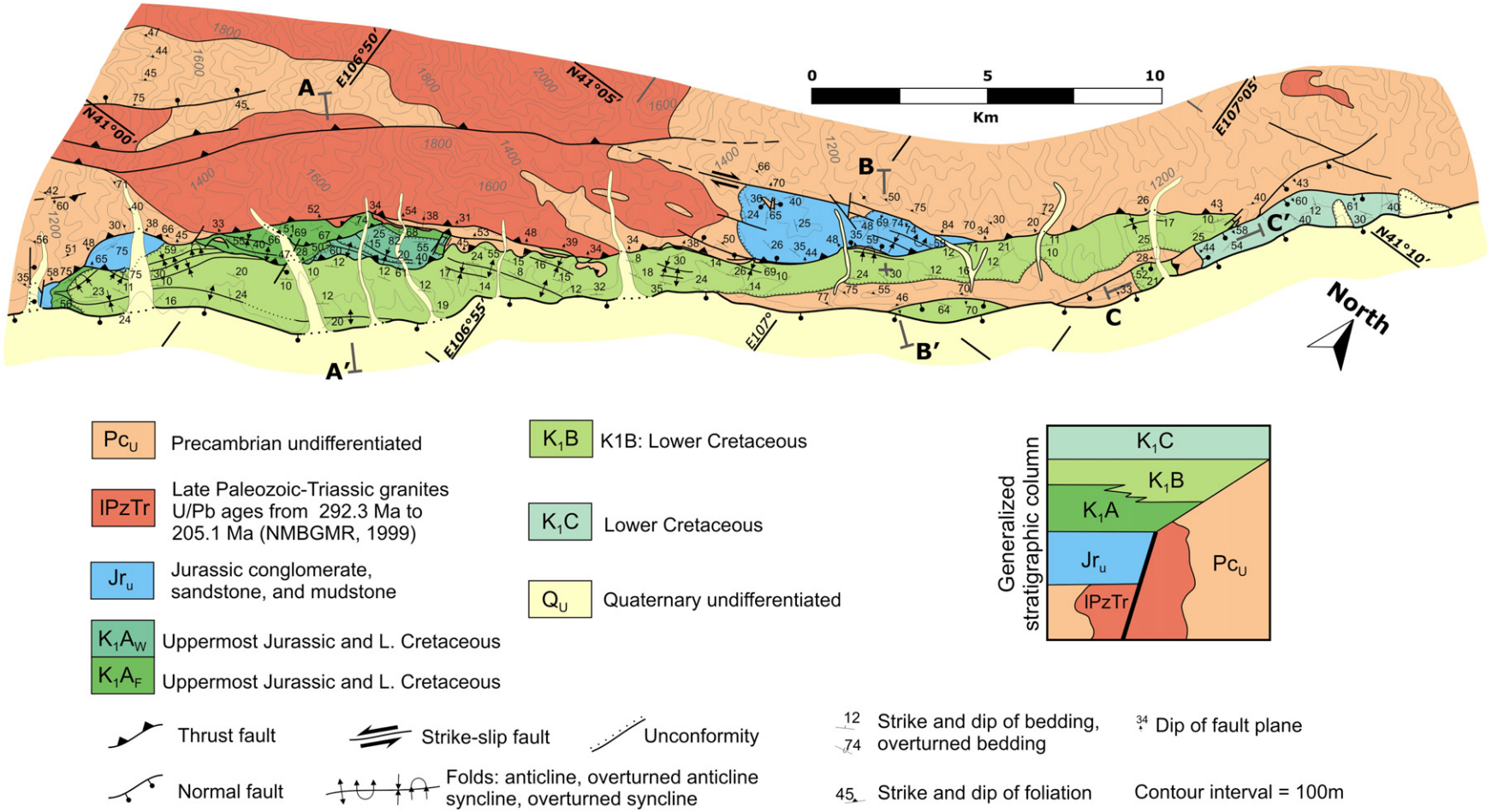

Fig. 2. Simplified geologic map of the south-central Lang Shan fold-thrust belt. Original mapping conducted at a scale of 1:25,000. Contact the corresponding author for a 1:50,000 version of this map. Unit ages from NMBGMR (1999), topography from SRTM data. Contour interval is 100 m. Note that ''north'' is to the upper right corner of the map.

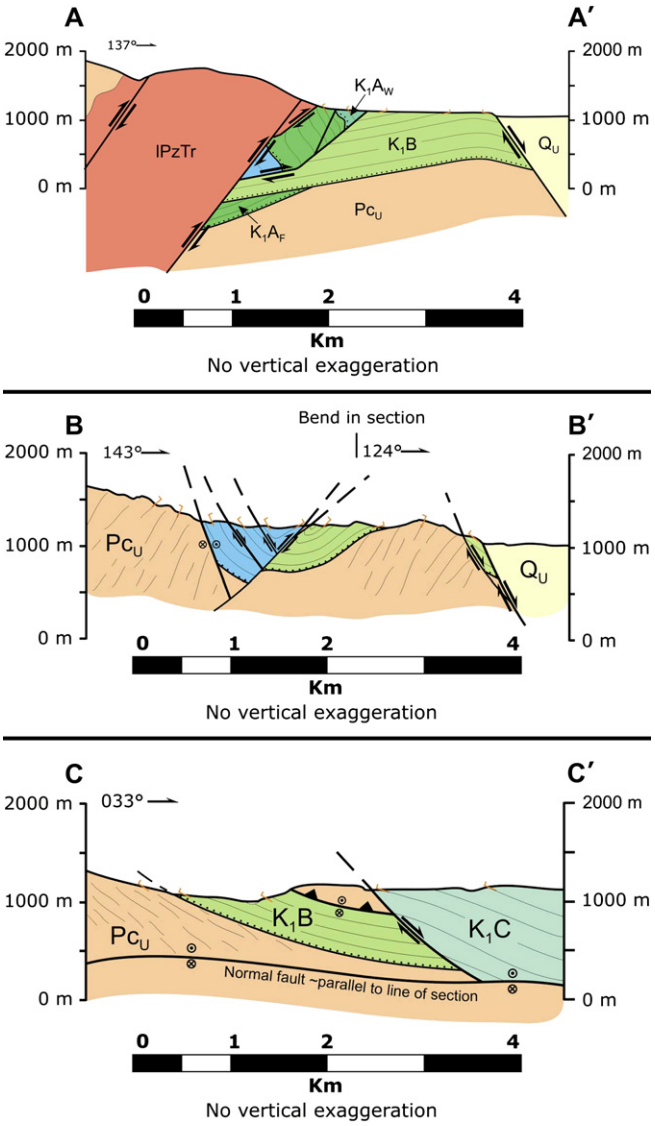

Fig. 3. Cross-sections from the south-central Lang Shan. See Fig. 2 for locations. Colors and units match Fig. 2. Orange lines at the surface are dip tadpoles (for interpretation of the color in the text, the reader is referred to the web version of the article).

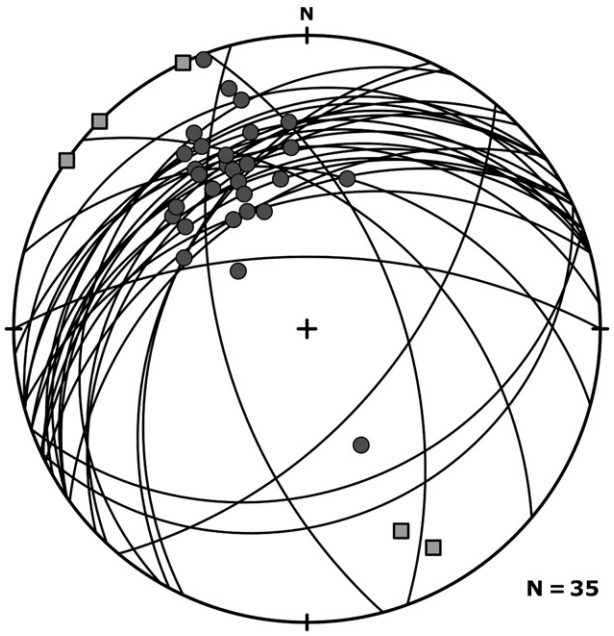

Fig. 4. Equal area, lower hemisphere stereoplot of data collected in the vicinity of cross-section AA′ (Fig. 2). Black lines represent fault planes, black dots represent striae measurements in fault gouge or on fault planes, and grey squares represent poles to axial planes. Average shortening direction is NNW–SSE (154°–334°).

on Fig. 3 (AA′–CC′). Section AA′ (Figs. 2, 3), displays the best example of the complex assortment of structures preserved in the fold-thrust belt. Striae measured on thrust fault planes and poles to axial planes of folds in the vicinity of cross-section AA′ (Figs. 2, 3) suggest an NNW–SSE shortening direction (Fig. 4).

The most prominent structure on the cross-sections and on the geologic map is a steep, northwest-dipping reverse fault that juxtaposes crystalline units against a variety of footwall units, most of which are Lower Cretaceous in age. In the vicinity of section AA′ (Figs. 2, 3) hanging wall, late Paleozoic – Triassic granites (U–Pb zircon ages range from 292.3 to 205.1 Ma; NMBGMR, 1999) are juxtaposed against footwall Lower Cretaceous unit K_1A along a fault that dips ~52° to the northwest. Just to the northeast of section AA′, the footwall of the same steep reverse fault is a complex ~250 m wide shear zone that contains Precambrian metasedimentary units and some granitoids (Fig. 5A). The southeastern edge of the disrupted sheet is marked by a second reverse fault (dip ~48° northwest) that carries metasedimentary units across a footwall of unit K_1A and late Paleozoic granite. The granite Lower Cretaceous strata contact is a low-angle (~25°–30°) northwest-dipping thrust fault. This important fault is truncated by younger, structurally higher reverse faults here and along strike as shown on section AA′ (Figs. 2, 3, 5A).

Farther southeast on cross-section AA′, Cretaceous units K_1A and K_1B are separated by a thrust fault that dips ~28°–40° to the northwest and contains up to 4 m of green to black clay-rich, fault gouge (Figs. 2, 3, 5B). Field relationships document that this is the structurally lowest thrust fault currently exposed in the Lang Shan fold-thrust belt. As with the other low-angle thrust fault described above, this thrust fault is cut by a steep reverse fault ~2.5 km to the south of section AA′ (N40°59′, E106°49′; Fig. 2). Along strike from section AA′ ~2 km, this southernmost exposed thrust sheet contains a steep tear fault (N41°02′, E106°54′; Fig. 2) that separates Lower Cretaceous unit K_1A to the south from Precambrian metasedimentary units that include carbonate and quartzite to the north. The footwall of this thrust fault remains the same (unit K_1B) on either side of the tear fault and locally contains progressive unconformities. Northeast of the tear fault the thrust fault has variable dips (20°–65°) and thick gouge (up to 6 m) is common. Farther to the northeast (N41°03′, E106°57′), steep out-of-sequence reverse faulting cuts all low-angle thrust faults, and places Precambrian metasedimentary units and late Paleozoic–Triassic granites on top of unit K_1B.

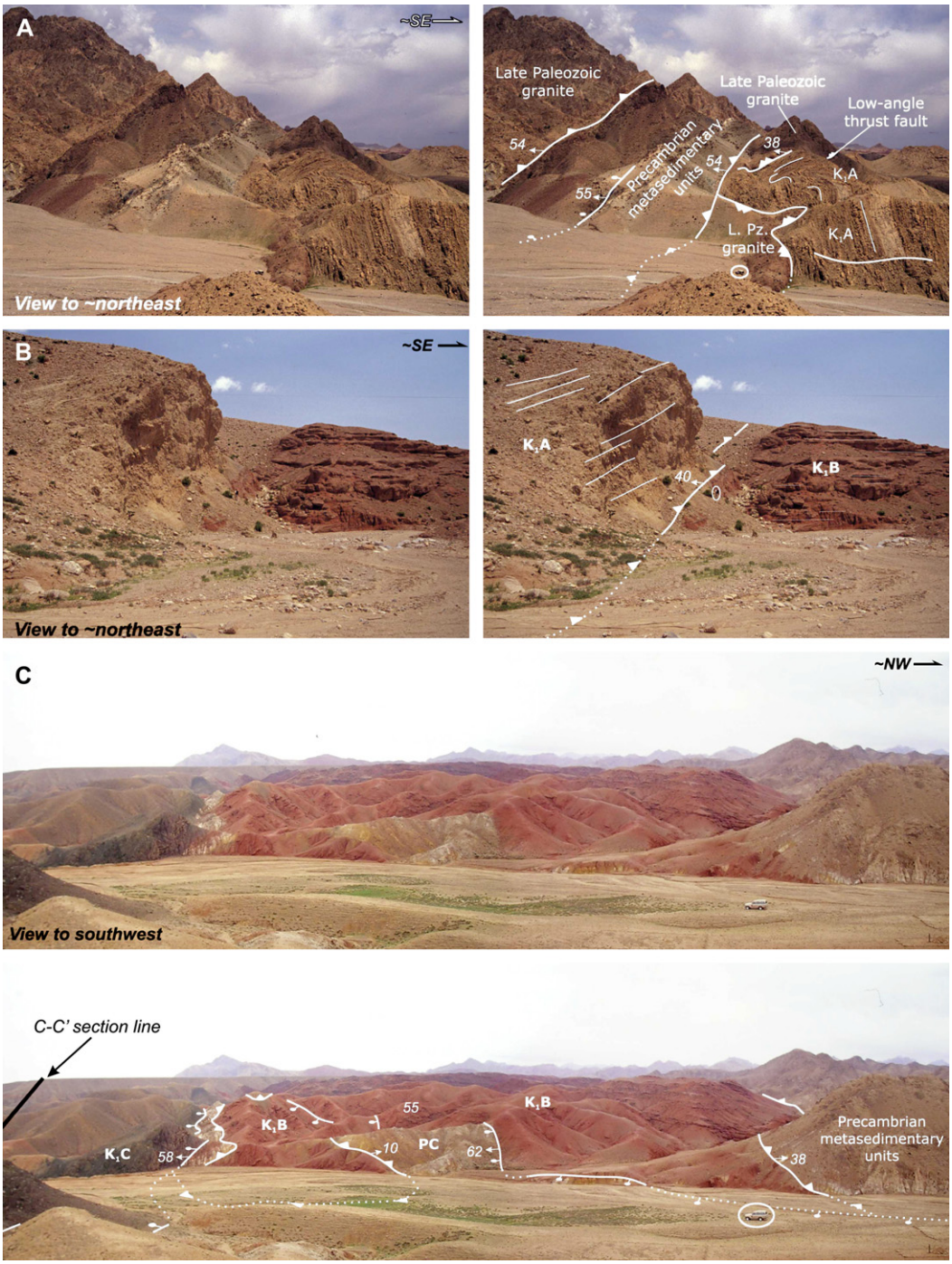

Fig. 5. (A) Shear zone at the northwestern end of ''Pig'' Canyon (Fig. 2). View to the northeast. Landcruiser circled for scale. A series of south–southeast directed steep reverse faults juxtapose crystalline units and truncate a low-angle thrust fault between Late Paleozoic granite and a Lower Cretaceous sedimentary unit. See text for details. (B) South–southeast directed thrust fault that juxtaposes Early Cretaceous sedimentary units, south-central Lang Shan. Up to 4 m of gouge is present along this fault. Person (circled) for scale. View to the northeast. (C) Excellent exposure of cross-cutting relationships in the northeastern portion of the study area, view to the southwest. A thrust fault places white/tan Precambrian metasedimentary units over red Cretaceous conglomerate and sandstone (unit K_1B) conglomerate and sandstone. The thrust sheet is cut by ~north-striking normal fault (center of image). Both the thrust fault and the north-striking normal fault are cut by a northeast-striking normal fault (left side of photo) with unit K_1C in the hanging wall. The approximate location of section CC′ (Fig. 3) is shown. Landcruiser circled for scale.

Near section BB′, in the vicinity of the triangular-shaped exposure of Jurassic strata, a northwest-dipping thrust fault (26°–48°) separates hanging wall Jurassic strata and a sliver of Precambrian marble from Lower Cretaceous unit K_1B in the footwall (Figs. 2, 3, BB′). A small footwall syncline (wavelength of ~20 m) can be found locally beneath the contact. Jurassic strata and Precambrian marble in the upper plate of the thrust fault are separated by northwest-dipping (45°–85°) normal fault, which is cut by the younger thrust. This northwest-dipping normal fault is syndepositional with respect

to Jurassic strata as carbonate breccias in the Jurassic section coarsen and thicken towards the normal fault. Jurassic strata in the south-central Lang Shan (ca. N41°05′, E107°) are bordered along their northern margin by an east–northeast trending dextral strike-slip fault (Fig. 2). The steep fault zone dips both north and south and displays sub-horizontal to west-plunging striae. Kinematic indicators such as tension cracks on fault planes suggest dextral, north-side-up slip. The fault juxtaposes Jurassic boulder conglomerate against Precambrian gneiss (north wall) and is cut by a thrust fault a few kilometers to the northeast of section BB′ (Fig. 2; N41°06.5′, E107°01′). The lower three-fourths of the Jurassic section is highly disrupted by small faults and shear bands. In contrast, the uppermost portion of the section, which is much finer grained, contains fewer faults and is apparently not nearly as disrupted. The entire Jurassic section is folded about east–northeast trending hinges.

In the northeastern-most portion of the field area, the same thrust fault that truncates low-angle thrust sheets in the vicinity of section AA′ (Figs. 2, 3), juxtaposes undifferentiated Precambrian units that include quartzite, marble, and a leucocratic muscovite-bearing pluton, against footwall K_1B conglomerate and sandstone (Fig. 5C). The fault is well exposed, dips ~35° to the northwest, and is easy to find because of the color contrast across it (red footwall vs. white/buff/tan hanging wall). Several ~north-striking normal faults offset the thrust fault (Figs. 2, 5C; N41°09′, E107°06′). The smaller down-to-the east normal fault shown in Fig. 5C is cut by a later northeast-trending, southeast-dipping normal fault that carries the youngest Lower Cretaceous unit, K_1C, in its hanging wall. The western margin of unit K_1C is an ~north-striking, 44° east-dipping normal fault (Fig. 3, CC′). The footwall of this fault is the upper plate of the low-angle thrust fault that has been displaced by northeast-striking normal faults (Fig. 2). It is important to note that unit K_1C, unlike all older units, is not cut by any thrust/reverse faults. Additional normal faults can be found throughout the field area and they have similar orientations as those described above: either north–northwest trending (e.g. the southwestern portion of the study area) or northeast trends that are sub-parallel to the active mountain-front normal fault (e.g. Fig. 3, BB′).

4. Timing relationships and structural chronology

The proposed chronology of events is based on cross-cutting relationships (Figs. 2, 3) and is presented in Fig. 6. Jurassic strata preserved in the south-central Lang Shan rest unconformably on the Precambrian basement (Fig. 2). The triangular-shaped exposure is bound along its southeast margin by normal and thrust faults and by a right-lateral strike-slip fault along its northern margin (Figs. 2, 3, 6). Jurassic strata fine upwards and may be syndepositional with respect to the right-lateral strike-slip fault along their northwestern margin and are syndepositional with respect to the north-dipping normal fault along their southern margin (Fig. 6; event 1). If this syndepositional interpretation is correct, then this exposure represents a structurally confined transtensional basin, and the strike-slip fault and normal fault are synchronous and structurally related. In any case, the dextral strike-slip fault and Jurassic normal fault are cut by a thrust fault that juxtaposes basement and these folded Jurassic strata in the hanging wall, against a Lower Cretaceous footwall (Fig. 2).

Cretaceous unit K_1A overlies an unconformable contact with Jurassic strata in the southwestern portion of the field area (Figs. 2, 6; event 2). Cretaceous unit K_1B was deposited unconformably on both unit K_1A and Precambrian metasedimentary basement units (Figs. 2, 6; event 3), which suggests either local erosion of unit K_1A prior to deposition of K_1B, or a time-transgressive basal unconformity to Lower Cretaceous units. The presence of progressive and buttress unconformities within the older two Cretaceous units (K_1A, K_1B), their local sediment sources, and coarsening upwards

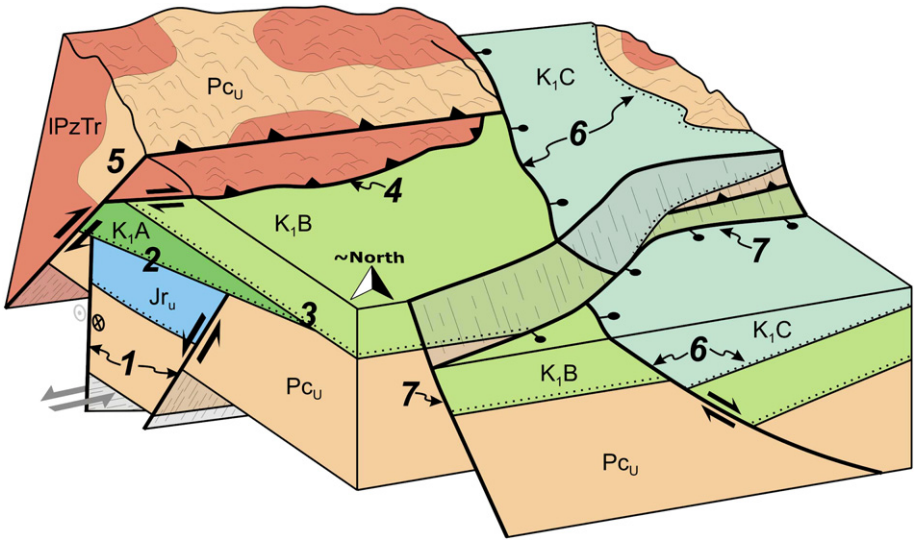

Fig. 6. Block model showing relative timing of cross-cutting relationships and structural development in the south-central Lang Shan. Colors are the same as Fig. 2 (for interpretation of the color in the text, the reader is referred to the web version of the article). Numbers represent deformational events discussed in the text.

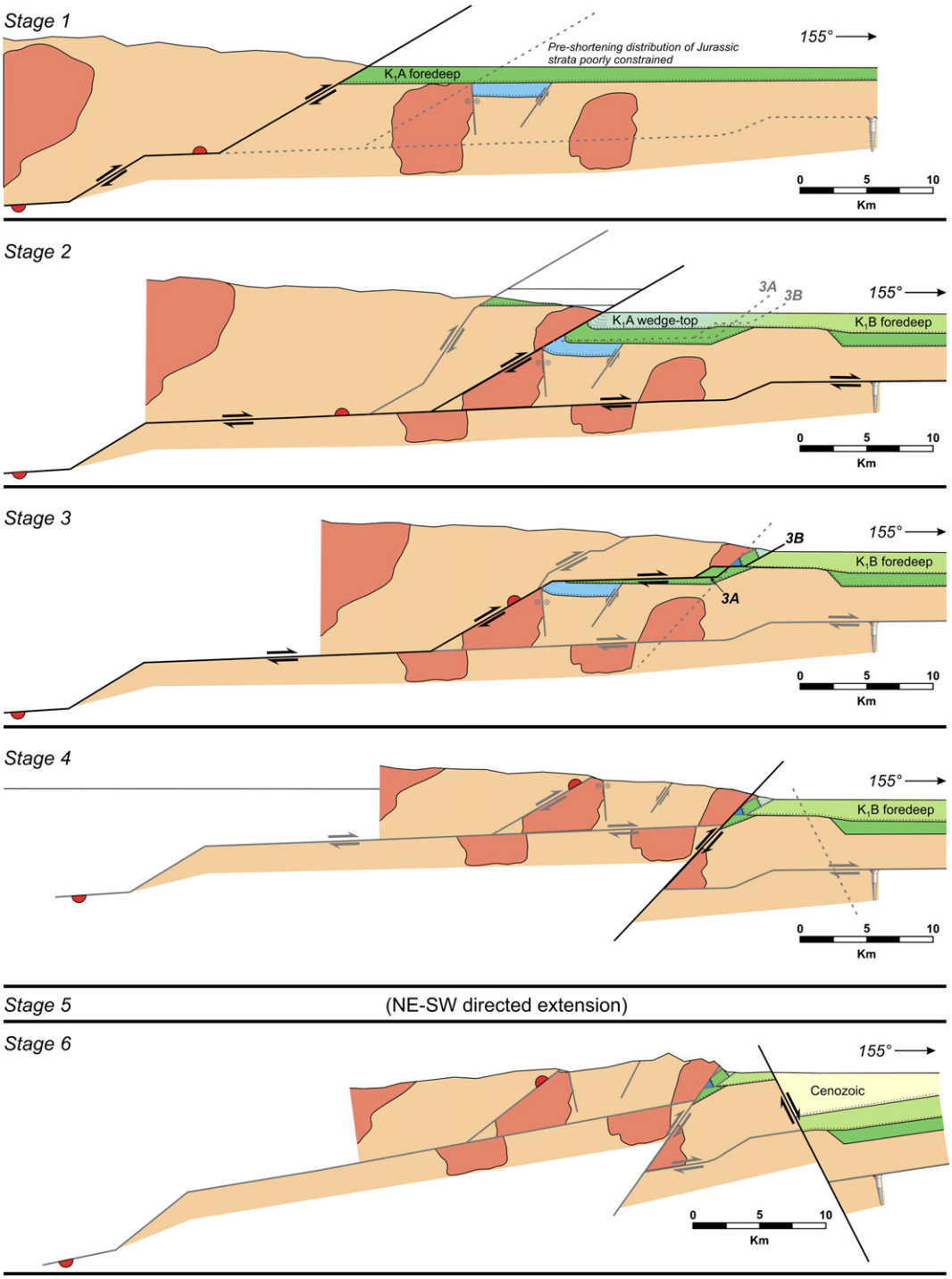

Fig. 7. Sequential development of the Lang Shan fold-thrust belt from the Late Jurassic to Recent. Note that plutons are shown schematically as their subsurface distribution is unknown. Red half-circles illustrate approximate displacement (for interpretation of the color in the text, the reader is referred to the web version of the article). Screw represents foreland pin. Northwest–southeast shortening is estimated at several tens of kilometers.

character suggests that they are synorogenic with respect to the fold-thrust belt. Thus, the Lang Shan fold-thrust belt was certainly active during the Early Cretaceous and Latest Jurassic. However, the initiation age of Lang Shan fold-thrust belt deformation is difficult to constrain because sedimentary units related to the earliest history of the thrust belt are now absent or unexposed.

The Lang Shan fold-thrust belt in the vicinity of cross-sections AA′ contains at least five major thrust sheets (Fig. 2). The stack of thrust sheets and their emplacement sequence is defined by the relative position of each sheet and cross-cutting relationships. We suspect that a large amount of shortening was accommodated by the Lang Shan fold-thrust belt given that all low-angle thrust sheets (Fig. 6; event 4),

carry different assemblages and the presence of thick synorogenic deposits.

Following fold-thrust belt deformation, there are at least two extensional events. The first episode occurs along north-to-northwest trending faults, with the largest in the northeastern portion of the field area (Figs. 2, 3, section CC′). While the exposure of this structure is spatially limited, important relationships are preserved. The hanging wall of this east-dipping normal fault contains Cretaceous unit K_1C, which is not cut by any thrust fault. We interpret unit K_1C as a synextensional sedimentary section initially bound by a normal fault along the basin's western margin (Fig. 6; event 6). This extension direction (east–west to northeast–southwest) is significantly different from northwest–southeast Early Cretaceous extension throughout much of northern China and Mongolia (Zheng et al., 1991, 1996; Webb et al., 1999; Graham et al., 2001; Davis et al., 2002; Ren et al., 2002; Meng et al., 2003; Darby et al., 2004; Johnson, 2004).

Extension also occurred along northeast-trending structures such as the mountain-front normal fault (Fig. 2). Additionally, in the northeast portion of the field area, a southeast-dipping normal fault cuts both a low-angle thrust fault and the north-to-northwest trending normal fault related to the first extensional event described above (Figs. 2, 6; events 6, 7). Locally, the southeast-dipping normal faults not along the range front offset Cenozoic pediments by a few meters. It is unclear if these faults are originally Mesozoic in age and related to regional northwest–southeast extension (e.g. Zheng et al., 1991, 1996; Webb et al., 1999; Graham et al., 2001; Davis et al., 2002; Ren et al., 2002; Meng et al., 2003; Darby et al., 2004; Johnson, 2004), and were reactivated in the Cenozoic, or if they are related to active extension (Fig. 6; event 7) along the southeast-dipping, mountain-front normal fault (e.g. Zhang et al., 1998).

5. Thrust belt evolution and reconstruction

We present a reconstruction (Fig. 7) that represents the evolution of the Lang Shan from initiation of crustal shortening (Late Jurassic (?)) through active extension along the mountain-front based upon the geology along cross-section AA′ (Figs. 2, 3). Unraveling the kinematic history of the Lang Shan fold-thrust belt is complicated by late, steep reverse faulting that uplifted the hinterland portion of low-angle thrust sheets and by subsequent crustal extension. However, cross-cutting relationships as well as hanging wall and footwall cutoffs preserved in the field area provide insights into the relative timing of deformation and synorogenic deposition that allow stepwise reconstruction. The initial conditions and pre-fold-thrust belt distribution of Jurassic strata and late Paleozoic–Triassic plutons in the Lang Shan are poorly constrained. Topography shown on the reconstruction (Fig. 7) is schematic.

The first stage in our reconstruction is largely based upon foreland basin strata (K_1A_F) preserved in the field area with cyclical provenance changes related hanging wall motion over ramp-flat geometries in the hinterland. The basin-bounding thrust fault shown in Stage 1 (Fig. 7) was not identified in the field area, but may be one of the crystalline on crystalline thrust contacts mapped in the rugged internal portion of the Lang Shan. Therefore, the displacement magnitude at this stage is unknown and has been schematically estimated at over 10 km—enough to generate a flexural load. We know that initial shortening in the thrust belt generated a load sufficient to produce a foreland basin with a minimum thickness of ~800 m. Additionally, the relatively fine-grained nature of the currently exposed lower portion of unit K_1A_F suggests that it was not deposited immediately adjacent to the thrust front.

Stage 2 (Fig. 7) deformation includes forward propagation of the thrust belt and continued development of the foreland basin. Key features of this stage include the deposition of the wedge-top portion of unit K_1A (K_1A_W), uplift and erosion of the lower portion of the K_1A_F in two locales along the reconstruction, and deposition of unit K_1B. From a structural standpoint, two faults are interpreted to have been active during this stage. The ~30° northwest-dipping, basin-bounding structure is presently exposed in the field area (Figs. 2, 5A) and truncates both Jurassic strata and Lower Cretaceous strata including proximal, coarse wedge-top conglomerate. The currently exposed upper plate of the thrust sheet is entirely composed of granitoids but clast composition of the wedge-top facies suggests recycling of older clastic sedimentary units combined with a granitic source terrane. The large fault-bend fold in the frontal portion of Stage 2 is an interpretation based upon observed cross-cutting relationships. Unit K_1B was deposited on both unit K_1A and crystalline basement (Fig. 2). This requires at least local uplift and erosion of older units prior to deposition of unit K_1B, which was accomplished by displacing the upper plate over a ramp-flat geometry, producing a broad anticline above which unit K_1B was deposited. Shortening accommodated during Stage 2 deformation is estimated at ~10 km. This estimate, as with others, was by determining the minimum amount of slip on the faults in the restoration to produce the relationships presently exposed in the study area.

The final low-angle thrust sheet emplaced in the reconstruction is shown in Stage 3. This thrust fault juxtaposes the lower portion of the wedge-top section (K_1A_W) along with older units and thrust faults on top of unit K_1B (Fig. 5B). The exposed relationships require two phases of shortening during Stage 3 deformation, the second of which is out-of-sequence (3B). The out-of-sequence thrust fault (3B) bypasses the original upper ramp (Fig. 7) by developing a new, near-surface, ramp-flat ramp system. This sequence of events provides a feasible solution to complicated juxtaposition of disparate synorogenic sedimentary sections (K_1A and K_1B), while maintaining the observed distribution and geometric arrangement of units and structures. Stage 3 deformation accounts for ~14 km of shortening in the Lang Shan fold-thrust belt.

Steep reverse faulting dominates Stage 4 (Fig. 7) deformation. The amount of displacement shown on the reconstruction (~5 km) was calculated by projecting the currently exposed base of the Jurassic section southwest to cross-section line AA′ (the restored section), which results in a minimum displacement. Following Stage 4 is northeast–southwest directed crustal extension—essentially perpendicular to the plane of the restoration. Therefore, no attempt was made to show this

post-shortening, Early Cretaceous extension. The last stage (6) of deformation on the restoration is extension along the mountain-front normal fault (Fig. 7).

6. Discussion and conclusions

The Lang Shan has a complicated Mesozoic to recent history of intraplate deformation that is constrained by well-exposed cross-cutting relationships. Deformation began with right-lateral strike-slip faulting and basin development along east-striking structures (Figs 2, 6) in the Early(?) Jurassic. Total right-lateral displacement is unknown. Following strike-slip deformation, the south-central Lang Shan underwent Late Jurassic–Early Cretaceous north–northwest—south–southeast shortening that accommodated a minimum of 40 km of displacement on both low-angle and steeply dipping thrust faults (Figs. 2–7). This intraplate deformation may be the result of far-field plate interaction such as subduction and collision of the Lhasa block along the southern margin of Eurasia in Jurassic–Cretaceous time (Dewey et al., 1988; Kapp et al., 2003), and reactivation of pre-existing weaknesses (e.g. Darby et al., 2001; Darby and Ritts, 2002).

Subsequently, the Lang Shan has experienced two extensional events (Figs. 2, 3, 5–7). The first was accommodated by ~north–south striking normal faults that cut slightly older thrust faults and produced an Early Cretaceous (NMBGMR, 1999) basin with a thickness of at least 500 m (Figs. 2, 3, 5, 6). This extension direction is enigmatic compared to regional northwest–southeast Early Cretaceous extension (Zheng et al., 1991, 1996; Webb et al., 1999; Graham et al., 2001; Davis et al., 2002; Ren et al., 2002; Meng et al., 2003; Darby et al., 2004; Johnson, 2004). Reasons for Early Cretaceous extension are highly controversial and include post-orogenic collapse, Pacific margin back-arc extension, and escape tectonics associated with collision along the southern margin of Asia (Watson et al., 1987; Traynor and Slayden, 1995; Davis et al., 1996, 2001, 2002; Yin and Nie, 1996; Zorin, 1999; Graham et al., 2001; Meng et al., 2003). We suspect that ~east–west extension in the Lang Shan represents gravitational collapse of a thickened crust and the interaction between the rigid and stable Ordos block (Darby and Ritts, 2002) and the surrounding poly-deformed crust (Darby et al., 2001). The youngest deformational event is the development of the mountain-front normal and associated sub-parallel structures. This system of normal faults, part of the Ordos graben system (e.g. Zhang et al., 1998), may be linked to left-lateral strike-slip faulting beyond the northern margin of the Tibetan Plateau and therefore be consequence of the collision between India and Asia (Darby et al., 2005).

Acknowledgements

We acknowledge NSF grant EAR-9903012 (awarded to G.A. Davis, USC) and EAR-0604443 (to BDR) donors of the Petroleum Research Fund, administered by the American Chemical Society (#38900-B8 to BDR), Louisiana State University and the Geological Society of America for providing financial support of this research.

The manuscript benefited greatly from discussions with G.A. Davis. Adrian Berry and Lynde Nanson provided excellent field assistance. Li Tianbin, Gao Yu, and others from the Ningxia Bureau of Geology and Mineral Resources provided excellent logistical support and technical advice. We thank Ken Ridgway and Delores Robinson for their helpful reviews and Bill Dunne for serving as Editor.

References

Cope, T., Ritts, B.D., Darby, B.J., Fildani, A., Graham, S., 2005. Carboniferous-Permian sedimentation on the northern margin of North China: implications for regional tectonics and climate change. International Geology Review 47, 270–296.

Darby, B.J., Davis, G.A., Zheng, Y., 2001. Structural evolution of the southwestern Daqing Shan, Yinshan belt, Inner Mongolia, China. In: Hendrix, M.S., Davis, G.A. (Eds.), Paleozoic and Mesozoic Tectonic Evolution of Central and Eastern Asia: From Continental Assembly to Intracontinental Deformation, vol. 194. Geological Society of America Memoir, pp. 199–214.

Darby, B.J., Ritts, B.D., 2002. Mesozoic contractional deformation in the middle of the Asian tectonic collage: the intraplate Western Ordos fold-thrust belt, China. Earth and Planetary Science Letters 205, 13–24.

Darby, B.J., Davis, G.A., Wang, X., Wu, F., Wilde, S., Yang, X., 2004. The Waziyu metamorphic core complex, Yiwulü Shan, Liaoning, China: timing and significance of high-strain crustal extension. Earth Science Frontiers 11, 145–155.

Darby, B.J., Ritts, B.D., Yue, Y., Meng, Q., 2005. Did the Altyn Tagh fault extend beyond the Tibetan Plateau? Earth and Planetary Science Letters 240, 425–435.

Davis, G.A., Xianglin, Qian, Yadong, Zheng, Heng-Mao, Tong, Cong, Wang, Gehrels, G.E., Shafiquallah, Muhammad, Fryxell, J.E., 1996. Mesozoic deformation and plutonism in the Yunmeng Shan: a metamorphic core complex north of Beijing, China. In: An, Yin, Harrison, T.M. (Eds.), The Tectonic Evolution of Asia. Cambridge University Press, pp. 253–280.

Davis, G.A., Darby, B.J., Zheng, Y., Spell, T., 2002. Geometric and temporal evolution of an extensional detachment fault, Hohhot metamorphic core complex, Inner Mongolia, China. Geology 30, 1003–1006.

Davis, G.A., Yadong, Zheng, Cong, Wang, Darby, B.J., Changhou, Zhang, Gehrels, G.E., 2001. Tectonic evolution of the Mesozoic Yanshan Fold and thrust belt, Northern China. In: Hendrix, M.S., Davis, G.A. (Eds.), Paleozoic and Mesozoic Tectonic Evolution of Central and Eastern Asia: From Continental Assembly to Intracontinental Deformation, vol. 194. Geological Society of America Memoir, pp. 171–197.

DeCelles, P.G., Giles, K.A., 1996. Foreland basin systems. Basin Research 8, 105–123.

Dewey, J.F., Shackleton, R.M., Chang, C., Sun, Y., 1988. Tectonic evolution of the Tibetan plateau. Philosophical Transactions of the Royal Society of London A327, 379–413.

Graham, S., Hendrix, M.S., Johnson, C.L., Badamgarav, D., Badarch, G., Amory, J., Porter, M., Barsbold, R., Webb, L.E., Hacker, B.R., 2001. Sedimentary record and tectonic implications of Mesozoic rifting in southeast Mongolia. Geological Society of America Bulletin 113, 1560–1579.

Gordon, R.G., 1998. The plate tectonic approximation: Plate nonrigidity, diffuse plate boundaries, and global plate reconstructions. Annual Reviews of Earth and Planetary Science 26, 615–642.

Hand, M., Sandiford, M., 1999. Intraplate deformation in central Australia, the link between subsidence and fault reactivation. Tectonophysics 305, 121–140.

Hendrix, M.S., Davis, G.A. (Eds.), 2001. Paleozoic and Mesozoic tectonic evolution of central and eastern Asia; from continental assembly to intracontinental deformation. Geological Society of America Memoir, 194, 447 pp.

Hendrix, M.S., Graham, S.A., Carroll, A.R., Sobel, E.R., McKnight, C.L., Schulein, B.J., Wang, Z., 1992. Sedimentary record and climatic

implications of recurrent deformation in the Tian Shan: evidence from Mesozoic strata of north Tarim, south Juggar, and Turpan basins, northwest China. Geological Society of America Bulletin 104, 53–79.

Johnson, C.L., 2004. Polyphase evolution of the East Gobi basin: sedimentary and structural records of Mesozoic–Cenozoic intraplate deformation in Mongolia. Basin Research 16, 79–99.

Kapp, P., Murphy, M.A., Yin, A., Harrison, T.M., Ling, D., Guo, J., 2003. Mesozoic and Cenozoic tectonic evolution of the Shiquanhe area of western Tibet. Tectonics 22, 1–23, doi:10.1029/2001TC001332.

Kluth, C.F., 1986. Plate tectonics of the Ancestral Rocky Mountains. In: Peterson, J.E. (Ed.), Paleotectonics and Sedimentation in the Rocky Mountain Region, United States, vol. 41. American Association Petroleum Geology Memior, pp. 353–369.

Meng, Q.R., Hu, J.M., Jin, J.Q., Zhang, Y., Xu, D.F., 2003. Tectonics of the late Mesozoic wide extensional basin system in the China–Mongolia border region. Basin Research 15, 397–416.

Nei Mongol Bureau of Geology and Mineral Resources (NMBGMR), 1991. Regional Geology of Nei Mongol Autonomous Region. Geological Publishing House, Beijing.

Nei Mongol Bureau of Geology and Mineral Resources (NMBGMR), 1999. Regional Geology of Nei Mongol Autonomous Region. Geological Publishing House, Beijing.

Ren, J., Tamakib, K., Lia, S., Zhang, J., 2002. Late Mesozoic and Cenozoic rifting and its dynamic setting in Eastern China and adjacent areas. Tectonophysics 344, 175–205.

Ritts, B.D., Darby, B.J., Cope, T., 2001. Early Jurassic extensional deformation and basin formation in the Yinshan belt, northern North China Block. Tectonophysics 339, 235–253.

Ritts, B.D., Hanson, A.D., Darby, B.J., Nansen, L., Berry, A.K., 2004. Sedimentary record of Triassic intraplate extension in North China: evidence from the nonmarine NW Ordos Basin, Helan Shan and Zhuozi Shan. Tectonophysics 386, 177–202.

Sandiford, M., Hand, M., 1998. Controls on the locus of intraplate deformation in central Australia. Earth and Planetary Science Letters 162, 97–110.

Shaw, R.D., Etheridge, M.A., Lambeck, K., 1991. Development of the late Proterozoic to mid-Palaeozoic intracratonic Amadeus Basin in central Australia: a key to understanding tectonic forces in plate interiors. Tectonics 10, 688–721.

Teyssier, C., 1985. A crustal thrust system in an intracratonic environment. Journal of Structural Geology 7, 689–700.

Watson, M.P., Hayward, A.B., Parkinson, D.N., Zhang, Z.M., 1987. Plate tectonic history, basin development and petroleum source rock deposition onshore China. Marine and Petroleum Geology 4, 205–225.

Webb, L.E., Graham, S.A., Johnson, C.L., Badarch, G., Hendrix, M.S., 1999. Occurrence, age, and implications of the Yagan-Onch Hayrhan metamorphic core complex, southern Mongolia. Geology 27, 143–146.

Webb, L.E., Johnson, C.L., 2006. Tertiary strike-slip faulting in southeastern Mongolia and implications for Asian Tectonics. Earth and Planetary Science Letters 241, 323–335.

Wong, W.H., 1929. The Mesozoic orogenic movement in eastern China. Bulletin of the Geological Society of China 8.

Yin, A., Nie, S., 1996. A Phanerozoic palinspastic reconstruction of china and its neighboring regions. In: Yin, A., Harrison, T.M. (Eds.), Tectonic Evolution of Asia. Cambridge University Press, pp. 442–485.

Zhang, Y., Mercier, J., Vergély, P., 1998. Extension in the graben systems around the Ordos (China), and its contribution to the extrusion tectonics of south China with respect to Gobi-Mongolia. Tectonophysics 285, 41–75.

Zheng, Y., Wang, S.Z., Wang, Y.F., 1991. An enormous thrust nappe and extensional metamorphic core complex newly discovered in Sino–Mongolian boundary area. Science in China (Series B) 34, 1145–1154.

Zheng, Y., Zhang, Q., Wang, Y., Liu, R., Wang, S.G., Zuo, G., Wang, S.Z., Lkaasuren, B., Badarch, G., Badamgarav, Z., 1996. Great Jurassic thrust sheets in Beishan (North Mountains) – Gobi areas of China and southern Mongolia. Journal of Structural Geology 18, 1111–1126.

Ziegler, P.A., Cloetingh, S., van Wees, J.-D., 1995. Dynamics of intra-plate compressional deformation: the Alpine foreland and other examples. Tectonophysics 252, 7–59.

Ziegler, P.A., van Wees, J.D., Cloetingh, S., 1998. Mechanical controls on collision-related compressional intraplate deformation. Tectonophysics 300, 103–129.

Zorin, Y.A., 1999. Geodynamics of the western part of the Mongolia–Okhotsk collisional belt, Trans-Baikal region (Russia) and Mongolia. Tectonophysics 306, 33–56.